Characterization of Piezoelectric Ceramic Transducer for Accurate Acoustic Speed Measurement

H. Lin, K.A. Gillis, J.T. Zhang

H. Lin (✉) · J.T. Zhang

Division of Thermometry and Materials Evaluation, National Institute of Metrology (NIM), Beijing 100013, P.R. China.

e-mail: linhong@nim.ac.cn

K.A. Gillis

Process Measurements Division, National Institute of Standards and Technology (NIST), Maryland 20899, USA

e-mail: keith.gillis@nist.gov

Abstract In this paper, the piezoelectric ceramics mounted on the endplates of a cylindrical resonator were used as the source and detector for acoustic speed measurements. The perturbations of the longitudinal gas modes of the cavity due to the compliance of the diaphragms (10 mm diameter, 0.3 mm thick) and the attached transducers were estimated from first-order perturbation theory. The estimated fractional shifts of the resonance frequencies in argon caused by the source and detector were 0.07×10^{-6} at 0.1 MPa and 273.16 K. The high signal-to-noise ratio (up to 1×10^{4}) we obtained with these transducers makes them suitable for acoustic thermometry. Heat generated by dissipation in transducers is an important consideration. The dissipation that we measured in the source transducer was only $0.7\ \mu W$ at the working voltage (7 V) and frequency (1 kHz).

Keywords Acoustic thermometry · Acoustic speed · Transducer · Piezoelectric ceramic · Cylinder

1 Introduction

Acoustic thermometry is one of the most accurate ways to determine thermodynamic temperature and Boltzmann constant by measuring the acoustic resonance frequencies of diluted, high purity argon or helium in a gas-filled cavity [1-4]. The most promising way to determine the universal gas constant R and the Boltzmann constant k_B with relative uncertainty less than 1×10^{-6} is the acoustic thermometry which can fulfill the new definition of temperature unit – Kelvin (K) [5]. In order to achieve this uncertainty, the acoustic impedance of the transducer used to generate and detect the acoustic signal in the cavity need to be determined over the whole working frequency range. Piezoelectric ceramic is one of proper transducers which can improve signal-to-ratio for determining the resonance frequency with relative uncertainties of 1×10^{-6} or less.

Quinn [6, 7] measured the Boltzmann constant by using a variable-length cylinder resonator with the piezoelectric ceramic as the detector. One obvious merit of this procedure lays in its high signal-to-noise ratio which can remedy the low quality factor Q for the cylinder resonator. But this brings perturbations to the acoustic and temperature fields for the determination of acoustic speed and the Boltzmann constant.

In this paper, the piezoelectric ceramic was designed on a diaphragm of the resonance cavity to provide stable acoustic signal. The acoustic impedance, the frequency shift caused by the two transducers and the heat generated by the power dissipation were determined by the experimental and theoretical investigations for the piezoelectric ceramic. The results showed that the piezoelectric ceramic can be used for the acoustic thermometry and bring low perturbations.

2 Fundamental theory

Consider a circular diaphragm with radius a and thickness t that has been

machined into a plate as shown in Fig. 1. A piezoceramic disc is firmly attached to the underside of the diaphragm such that the strains in the piezoceramic are assumed to be equal to the strains in the diaphragm. A pressure difference Δp applied uniformly across the diaphragm will cause the diaphragm to deflect by an amount

$$z(r) = -\frac{3(1-v^2)a^4}{16t^3}\left(\frac{\Delta p}{Y}\right)\left[1-\left(\frac{r}{a}\right)^2\right]^2 \tag{1}$$

where Y is Young's modulus, ν is the Posson's ratio, and z is the deflection of the plate as a function of distance r from the axis [8]. Δp is defined as positive if the pressure above the diaphragm in Fig. 1 is greater than the pressure below the diaphragm. Eq. (1) describes a plate with a "clamped" boundary condition.

The average deflection over the area of the plate is:

$$\langle z\rangle = \frac{1}{\pi a^2}\int_0^a z(r)2\pi r dr = -\frac{(1-v^2)a^4}{16t^3}\left(\frac{\Delta p}{Y}\right). \tag{2}$$

The effective the compliance per unit area of the diagram, defined as

$$\chi = \frac{\langle z\rangle}{\Delta p} = -\frac{(1-v^2)a^4}{16t^3}\frac{1}{Y}, \tag{3}$$

is used to estimate the perturbation to the resonance frequencies in the next section.

The stresses in the diaphragm as a function of distance from the center due to an applied pressure are approximately [10]

$$\sigma_r = \frac{3}{8}\left(\frac{a}{t}\right)^2\left[(3+v)\left(\frac{r}{a}\right)^2-(1+v)\right]\Delta p \tag{4}$$

$$\sigma_\theta = \frac{3}{8}\left(\frac{a}{t}\right)^2\left[(1+3v)\left(\frac{r}{a}\right)^2-(1+v)\right]\Delta p \tag{5}$$

where σ_r and σ_θ are the radial and azimuthal stresses. The radial and azimuthal strains in the diaphragm are given by

$$\varepsilon_r = \frac{\partial u_r}{\partial r} = \frac{1}{Y}(\sigma_r - v\sigma_\theta) \tag{6}$$

$$\varepsilon_\theta = \frac{1}{r}\frac{\partial u_\theta}{\partial \theta}+\frac{u_r}{r} = \frac{1}{Y}(\sigma_\theta - v\sigma_r). \tag{7}$$

Similar relationships hold for the strains in the piezoceramic in terms of Young's

modulus Y_{PZT} and Poisson's ratio ν_{PZT}. We equate the radial strains and the azimuthal strains in the diaphragm and the ceramic, $\varepsilon_r = (\varepsilon_r)_{\mathrm{PZT}}$ and $\varepsilon_\theta = (\varepsilon_\theta)_{\mathrm{PZT}}$, where the subscript PZT refers to the piezoceramic. These relationships can be inverted to give relationships between the stresses in the ceramic and in the diaphragm,

$$(\sigma_r)_{\mathrm{PZT}} = \frac{Y_{\mathrm{PZT}}}{\left(1-\nu_{\mathrm{PZT}}^2\right)}\left[(\varepsilon_r)_{\mathrm{PZT}} + \nu_{\mathrm{PZT}}(\varepsilon_\theta)_{\mathrm{PZT}}\right] = \frac{Y_{\mathrm{PZT}}}{Y}\sigma_r \tag{8}$$

$$(\sigma_\theta)_{\mathrm{PZT}} = \frac{Y_{\mathrm{PZT}}}{\left(1-\nu_{\mathrm{PZT}}^2\right)}\left[(\varepsilon_\theta)_{\mathrm{PZT}} + \nu_{\mathrm{PZT}}(\varepsilon_r)_{\mathrm{PZT}}\right] = \frac{Y_{\mathrm{PZT}}}{Y}\sigma_\theta . \tag{9}$$

For a circular piezoelectric ceramic disc that has been poled along the *z*-axis (perpendicular to the flat faces), the relevant piezoelectric coefficients relate the stresses and strains to the electric fields

$$\frac{\Delta a_{\mathrm{PZT}}}{a_{\mathrm{PZT}}} = 2d_{31}E_z \qquad\qquad E_z = g_{31}\frac{F_r}{2\pi a_{\mathrm{PZT}} t_{\mathrm{PZT}}} \tag{10}$$

where F_r is the radial-component of the force, E_z is the electrical field in the z direction, d and g are the electro-mechanical properties matrices of piezoelectric ceramic. Eq. (10) is obtained from the constitutive equations.

We realized the piezoceramic-diaphragm system shown in Fig. 2 in the endplates of a cylindrical resonator. A very thin diaphragm (0.3 mm thick), axially located, was machined into each endplate. A piezoelectric ceramic disc was attached to the outer surface of each diaphragm with epoxy as shown in Fig. 2. One was used as an acoustic source and the other as a detector. The resonator was made from oxygen-free copper, had an inner radius of resonator of 40 mm, an inner length of 129.4 mm, and a wall thickness of 10 mm.

3 Source and detector

The model described in the section 1 was used to estimate the source strength and detector sensitivity of the PZT diaphragm transducers. The RMS volume displaced by the diaphragm is

$$\Delta V = \pi a^2 \langle z \rangle, \tag{11}$$

where a is the radius of the well on the endplate. For the longitude mode of the cylindrical resonator, the acoustic pressure $\tilde{p}_{\text{Long}}$ generated at resonance is

$$\tilde{p}_{\text{Long}} = 4iQ\rho c^2 \frac{\Delta V}{2V}, \tag{12}$$

where Q is the quality factor for the resonator and V is the volume of the resonator, and ρ and c are the density and speed of sound of gas in the resonator, respectively.

From Eq. (10), the radial strain in the diaphragm at $r = a_{\text{PZT}}$ is given by:

$$\left[\left(\varepsilon_r \right)_{\text{PZT}} \right]_{r=a_{\text{PZT}}} = \frac{\Delta a_{\text{PZT}}}{a_{\text{PZT}}} = \left(\varepsilon_r \right)_{r=a_{\text{PZT}}} \tag{13}$$

where a_{PZT} is the radius of the piezoelectric ceramic. The strain in the PZT due to the applied voltage produces in the diaphragm a similar strain, which we relate to an effective pressure that results in the diaphragm deflection. From Eqs. (4) and (5), we obtain the relationship between the strain generated in the diaphragm and the effective pressure Δp generated by the PZT

$$\left(\varepsilon_r \right)_{r=a_{\text{PZT}}} = \frac{1}{Y} \frac{3}{8} \left(\frac{a}{t} \right)^2 \Delta p \left(1 - v^2 \right) \left[3 \left(\frac{a_{\text{PZT}}}{a} \right)^2 - 1 \right]. \tag{14}$$

Combining Eqs. (10), (13) and (14), and also remembering $E_z = V_{\text{s}} / t_{\text{PZT}}$, we find the effective pressure

$$\Delta p = \frac{16}{3} \frac{d_{31} V_{\text{s}}}{t_{\text{PZT}}} \left(\frac{t}{a} \right)^2 Y \frac{1}{\left(1 - v^2 \right) \left[3 \left(\frac{a_{\text{PZT}}}{a} \right)^2 - 1 \right]}. \tag{15}$$

From Eqs. (2) and (15), we estimate the displaced volume ΔV

$$\Delta V = \pi a^2 \langle z \rangle = -\frac{\pi}{3} \frac{a^4}{t_{\text{PZT}} t} \frac{d_{31} V_{\text{s}}}{\left[3 \left(\frac{a_{\text{PZT}}}{a} \right)^2 - 1 \right]}. \tag{16}$$

Finally, we estimate the longitude acoustic pressure generated by the PZT source from Eq. (12) as a function of the applied voltage V_{s}

$$\tilde{p}_{\text{Long}} = -\frac{2iQ\rho c^2}{3R^2L}\frac{a^4}{t_{\text{PZT}}t}\frac{d_{31}V_{\text{s}}}{\left[3\left(\frac{a_{\text{PZT}}}{a}\right)^2-1\right]} \tag{17}$$

where R and L are the radius and length of the cylindrical resonator, respectively.

Next, we estimate the sensitivity of the detector. The radial stress for the PZT detector is

$$\left(\sigma_r\right)_{\text{PZT}} = \frac{Y_{\text{PZT}}}{Y}\sigma_r = \frac{Y_{\text{PZT}}}{Y}\frac{3}{8}\left(\frac{a}{t}\right)^2\left[\left(3+v\right)\left(\frac{r}{a}\right)^2-\left(1+v\right)\right]\Delta p\,. \tag{18}$$

The voltage from the detector is

$$\begin{aligned}\tilde{V} &= \left\langle E\right\rangle_{\text{PZT}} t_{\text{PZT}} = t_{\text{PZT}}\frac{1}{\pi a_{\text{PZT}}^2}\int_0^{a_{\text{PZT}}} g_{31}\left(\sigma_r\right)_{\text{PZT}} 2\pi r dr \\ &= t_{\text{PZT}} g_{31}\frac{Y_{\text{PZT}}}{Y}\frac{3}{16}\left(\frac{a}{t}\right)^2\tilde{p}\left[\left(3+v\right)\left(\frac{a_{\text{PZT}}}{a}\right)^2-2\left(1+v\right)\right]\end{aligned} \tag{19}$$

where $\tilde{p}$ is the RMS acoustic pressure. We combine Eqs. (17) and (19) to estimate the detector signal at a longitudinal resonance in the cylindrical cavity as a function of the RMS source voltage V_{s}

$$\tilde{V} = -g_{31}d_{31}V_{\text{s}}\frac{Y_{\text{PZT}}}{Y}\frac{iQ\rho c^2}{8}\frac{a^6}{t^3R^2L}\left[\left(3+v\right)\left(\frac{a_{\text{PZT}}}{a}\right)^2-2\left(1+v\right)\right]\left[3\left(\frac{a_{\text{PZT}}}{a}\right)^2-1\right]^{-1}. \tag{20}$$

4 Results and discussions

The piezoelectric ceramics used in this paper were type 402 from Piezo Kinetics Inc [9]. The properties of PZT 402 are shown in Table 1.

4.1 Location of the source and detector

For the steady state, the modified Helmholtz equation for forced oscillations of the acoustic pressure is [10] [11]

$$\nabla^2 \tilde{p}_{ac}\left(\mathbf{r},t\right) + k_{ac}^2 \tilde{p}_{ac}\left(\mathbf{r},t\right) = S_\omega\left(\mathbf{r}\right)e^{i\omega t}, \tag{21}$$

where $\tilde{p}$ is the acoustic pressure, $k_{ac} = \frac{\omega}{c} - i\alpha_b$, $S_\omega\left(\mathbf{r}\right)$ is the source strength, ω is the source frequency, and α_b is the bulk absorption coefficient. If the sound source

is embedded in the boundary wall at $\mathbf{r} = \mathbf{r_0}$ and drives the sound by a small motion of the boundary like a piston, then we may incorporate the source into the boundary condition and obtain the pressure response from

$$p_\omega(\mathbf{r}) = \int_V S_\omega(\mathbf{r}')\, G_\omega(\mathbf{r} \mid \mathbf{r}')\, dV' + i\omega\rho \int_S G_\omega(\mathbf{r} \mid \mathbf{r}')\, \hat{\mathbf{n}} \cdot \mathbf{u}_{\mathrm{src}}(\omega, \mathbf{r}')\, dS', \tag{22}$$

where G is the Green's function and $\mathbf{u}_{\mathrm{src}}$ is the source strength, respectively. There are no volume sources in our case, so the volume integral in Eq. (22) vanishes. To proceed, we expand the Green's function in the surface integral in terms of the eigenfunctions of Eq. (21) in the usual way [11].

The actual source and detector transducers are not point objects, but they are small compared to the wavelength of sound. The approximate the integral over the source in Eq. (22) by a uniform velocity and the average wavefunction at $\mathbf{r_0}$ $\left\langle \Psi_N(\mathbf{r_0}) \right\rangle_s$ over the area of the source. The signal from the detector transducer at $\mathbf{r_d}$ is proportional to the average of the acoustic pressure over the area of the detector. When we average both sides of Eq. (22), replace $\Psi_N(\mathbf{r_d})$ in the expanded Green's function with its average $\left\langle \Psi_N(\mathbf{r_d}) \right\rangle_d$. In terms of these average quantities, the detector signal is proportional to

$$\left\langle p_\omega(\mathbf{r}_d) \right\rangle_d \propto \sum_N \frac{if \left\langle \Psi_N(\mathbf{r}_d) \right\rangle_d \left\langle \Psi_N(\mathbf{r}_0) \right\rangle_s}{\Lambda_N \left(F_N^2 - f^2\right)}, \tag{23}$$

where Ψ is the eigenfunction and $\Lambda_N = (1/V)\int_V \Psi_N^2 dV$, F_N is the (complex valued) resonance frequency.

The eigenfunctions for the rigid-walled resonator are [10]

$$\Psi_{lmn}(\mathbf{r}) \propto J_m(\chi_{mn} r/R)\left[\cos(m\phi) + \sin(m\phi)\right]\cos(l\pi z/L) \tag{24}$$

where $l = 0, 1, 2, \ldots$ is the longitudinal quantum number, $m = 0, \pm 1, \pm 2, \ldots$ is the azimuthal quantum number, and $n = 0, 1, 2, \ldots$ is the radial quantum number. When $|m| > 0$, the eigenfunctions with azimuthal quantum numbers $\pm|m|$ are degenerated.

J_m is the cylindrical Bessel function and χ_{mn} is the turning point.

If the thermal and viscous boundary layer corrections are assumed to be the only perturbations, the acoustic pressure of the cylinder resonator is obtained from the first-order approximation of acoustic theory as [11]

$$\mathrm{Re}\left\langle p_\omega(\mathbf{r}_d)\right\rangle_d \propto f^3 \frac{\delta_T}{R}\sum_{lmn}\frac{A_{lmn}\Omega_{lmn}}{\left[f_{0,lmn}^2 - f^2\left(1+\frac{\delta_T}{R}\Omega_{lmn}\right)\right]^2 + \left(f^2\frac{\delta_T}{R}\Omega_{lmn}\right)^2} \tag{25}$$

$$\mathrm{Im}\left\langle p_\omega(\mathbf{r}_d)\right\rangle_d \propto f\sum_{lmn}\frac{A_{lmn}\left[f_{0,lmn}^2 - f^2\left(1+\frac{\delta_T}{R}\Omega_{lmn}\right)\right]}{\left[f_{0,lmn}^2 - f^2\left(1+\frac{\delta_T}{R}\Omega_{lmn}\right)\right]^2 + \left(f^2\frac{\delta_T}{R}\Omega_{lmn}\right)^2} \tag{26}$$

where

$$A_{lmn} = (-1)^l \frac{J_m(\chi_{mn}a/R)J_m(\chi_{mn}b/R)\left[\cos(m\phi_d)+\sin(m\phi_d)\right]}{\frac{1}{\delta_l}\left(1-\frac{m^2}{\chi_{mn}^2}\right)J_m^2(\chi_{mn})} \tag{27}$$

$$\Omega_{lmn} = \frac{(\gamma-1)}{1-\frac{m^2}{\chi_{mn}^2}}\left(1+\frac{R\varepsilon_l}{L}-\left(\frac{m}{\chi_{mn}}\right)^2\varepsilon_l\frac{R}{L}\right)+\frac{\sqrt{\mathrm{Pr}}}{1-\frac{m^2}{\chi_{mn}^2}}\left(1-\frac{\chi_{mn}^2-m^2}{\left(l\pi\frac{R}{L}\right)^2+\chi_{mn}^2}\left(1-\frac{R\varepsilon_l}{L}\right)\right) \tag{28}$$

where f_0 is the unperturbed resonance frequency, δ_T is the thickness of the thermal boundary layer, γ is the adiabatic index, Pr is the Prandtl number, $\varepsilon_0 = 1$ and $\varepsilon_{l>0} = 2$.

The theoretical response from Eqs. (25)-(28) predicts that the coupling between the transducers and a particular mode (and therefore the observed response) will be minimum (maximum) when the transducers are placed at a pressure node (antinode) for that mode. To test this prediction, we measured the acoustic spectrum of the cylindrical resonator (Fig. 2), filled with argon at 0.1 MPa and 293.16 K, with the source transducer placed at two different locations: (1) the center of the endplate, $(r,\phi,z) = (0,0,0)$, to maximize the coupling to the longitudinal and radial modes while minimizing the coupling to the azimuthal modes, and (2) off center at

$(r,\phi,z)=(0.628R,0,0)$, which is at a radial node for the modes (l,0,1) for l = 0,1,2,....

In both cases, the detector was located on axis at the opposite end of the resonator, i.e. $(r,\phi,z)=(0,0,L)$. Figure 3 shows the measured frequency response between 1 kHz and 6 kHz for case (1) with both transducers located on axis. The longitudinal modes (l,0,0), the radial mode (0,0,1), and the mixed modes (l,0,1) are clearly visible. The azimuthal modes near 2334 Hz, 3872 Hz, and 5326 Hz do not appear, since the coupling of these modes to both transducers is weak. Figure 4 shows the response for case (2) over the same frequency range as Fig. 3. The radial and mixed mode amplitudes have been reduced by a factor of 200 due to the reduced coupling. The azimuthal modes again do not appear since the coupling to the detector is weak.

4.2 Compliance and perturbation of the transducer

From Eq. (3), the compliance of the diaphragm χ is

$$\chi=\frac{\langle z\rangle}{\Delta p}=-\frac{\left(1-\nu^2\right)a^4}{16t^3}\frac{1}{Y} \tag{29}$$

The acoustic admittance of the transducers is

$$y_{\mathrm{tr}}=i\omega\rho c\chi \tag{30}$$

We use first-order perturbation theory to estimate the shift frequency for the longitude modes [12]

$$\frac{\Delta f_{\mathrm{tr}}}{f_0}=\frac{iy_{\mathrm{tr}}A_{\mathrm{tr}}}{l\pi^2R^2}=-\frac{i\rho c^2\chi A_{\mathrm{tr}}}{\pi R^2L} \tag{31}$$

Table 2 shows the estimated perturbations for 1/4 inch microphone and PZT 402 at 273.16 K and different pressures. The perturbations for microphone are calculated from Ref. [1] for a spherical resonator.

4.3 Heat generated by the PZT

Figure 5 shows the circuit we used to measure the dissipation factor tanδ as a function of voltage and frequency. The equivalent circuit for the PZT is assumed to be

a parallel combination of resistance R_1 and capacitance C_p, which is shown in the dash frame in Fig. 5. The voltage across PZT was measured by the lock-in SR830 and the PZT was attached on the endplate shown in Fig. 2. The R_0 (200.110 Ω) is a standard resistor which has very low capacity and induction. The power dissipation then can be determined by

$$P_{\text{diss}} = \frac{V_0}{R_0} V_{\text{PZT}} \tan\delta \tag{32}$$

Table 3 lists the results and the power dissipation for the PZT 402. Fig. 6 shows the power dissipation as a function of the square of source voltage V_s^2 at different frequency. If the PZT is operated at 7 V (RMS), the power dissipation will be 0.75~35 μW at 1~15 kHz by extrapolating from the values shown in Fig. 6.

4.4 Signal-to-noise ratio

The Piezoelectric ceramic transducers can improve the signal-to-noise ratio for the cylinder resonator. Figure 7 shows a typical acoustic resonance for which the resonance frequency was $F_N = f_N + ig_N = 1976.4072 + i1.7668$ Hz. Figure 8 shows the amplitude deviation for the in-phase and quadrature components. The signal-to-noise ratio is more than 1×10^4.

5 Conclusions

The piezoelectric ceramic transducer can be used for the acoustic thermometry to generate and detect the acoustic signal. The piezoelectric ceramic transducers were set on the middle of each endplate in order to minimize the coupling to the azimuthal modes. We observed a signal-to-noise ratio up to 1×10^4 for cylinder resonator which is high enough to fit the complex resonance frequency with a precision of 10^{-7} of f_N. The heat generated by the piezoelectric ceramic transducer is 0.75 to 35 μW when the voltage is 7 V and frequency is 1 to 15 kHz, respectively. The

perturbations to the acoustic field are only -0.03×10^{-6} and -0.27×10^{-6} when pressure is 0.1 MPa and 1 MPa, respectively, at 273.16 K in argon.

Acknowledgments This work was supported by the National Natural Science Foundation of China (No. 50906076) and the National Science & Technology Pillar Program (2006BAF06B00) in China.

References

1. M.R. Moldover, J.P.M. Trusler, T.J. Edwards, J.B. Mehl, J. Res. Natl. Bur. Stand. **93**, 85 (1988)
2. M.R. Moldover, S.J. Boyes, C.W. Meyer, A.R.H. Goodwin, J. Res. Natl. Inst. Stand. Technol. **104**, 11 (1999)
3. G. Benedetto, R.M. Gavioso, R. Spagnolo, P. Marcarino, A. Merlone, Metrologia **41**, 74 (2004)
4. L. Pitre, M.R. Moldover, W.L. Tew, Metrologia **43**, 142 (2006)
5. B. Fellmuth, C. Gaiser, J. Fischer, Meas. Sci. & Tech. **17**, R145 (2006)
6. T.J. Quinn, A.R. Colclough, T.R.D. Chandler, Philos. trans. R. Soc. Lond. A **283**, 367 (1976)
7. A.R. Colclough, T.J. Quinn, T.R.D. Chandler, Proc. R. Soc. Lond. A **368**, 125 (1979)
8. R.J. Roark, *Formulas for stress and strain*, 4th edn. (McGraw-Hill, New York, 1965)
9. In order to describe materials and experimental procedures adequately, it is occasionally necessary to identify commercial products by the manufacturer's name or label. In no instance does such identification imply endorsement by the National Institute of Metrology (NIM) or the National Institute of Standards and Technology (NIST); nor does it imply that the particular product or equipment is necessarily the best available for the purpose
10. J.P.M. Trusler, *Physical acoustics and metrology of fluids* (Hardcover, Bristol, 1991)
11. P.M. Morse, K.U. Ingard, *Theoretical Acoustics* (McGraw-Hill, New York, 1968)
12. K.A. Gillis, H. Lin, M.R. Moldover, J. Res. Natl. Inst. Stand. Technol. **114**, 263 (2009)
13. M.R. Moldover, J.B. Mehl, M. Greenspan, J. Acoust. Soc. Am. **79**, 253 (1986)

Figure Captions

Fig. 1 Pressure applied on a diaphragm

Fig. 2 Cylinder resonator and the transducers settlement

Fig. 3 Spectra for cylinder resonator at 1~6.5 kHz in argon when the source transducer is at $(r,\phi,z)=(0,0,0)$ and detector is at $(r,\phi,z)=(0,0,L)$

Fig. 4 Spectra for cylinder resonator at 1~6.5 kHz in argon when the source transducer is at $(r,\phi,z)=(0.628R,0,0)$ and detector is at $(r,\phi,z)=(0,0,L)$

Fig. 5 Circuit used to measure the dissipation factor

Fig. 6 Power dissipation of PZT 402 changing with the square of source voltage for different frequency

Fig. 7 The in-phase and quadrature voltages from the PZT detector as a function of frequency near the (100) longitude mode of cylinder resonator (2*R*=80 mm, *L*=80 mm) in argon.

Fig. 8 Measured voltages minus calculated voltages[13]

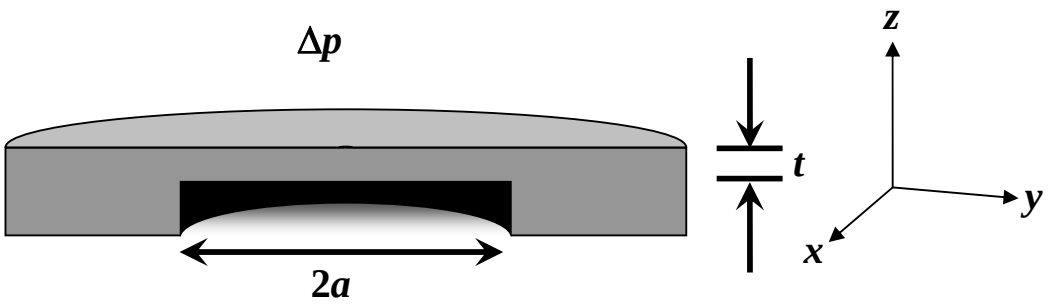

Fig. 1. Pressure applied on a diaphragm

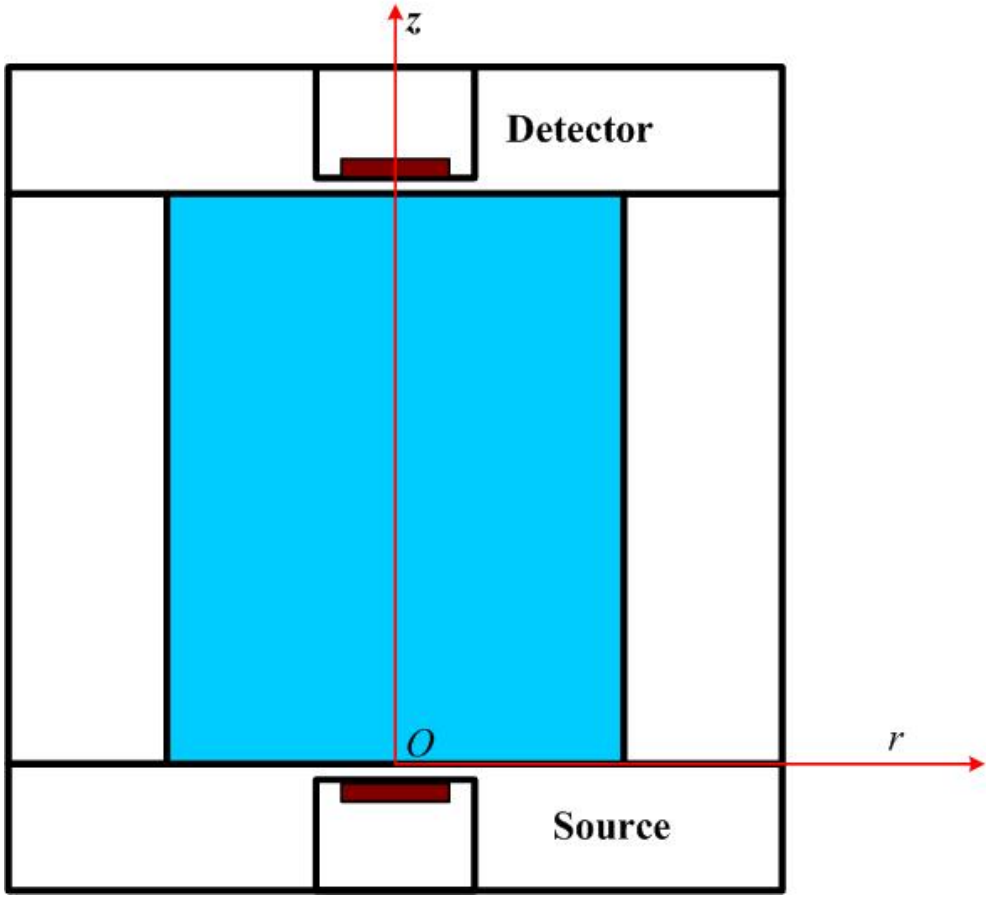

Fig. 2. Cylinder resonator and the transducers settlement

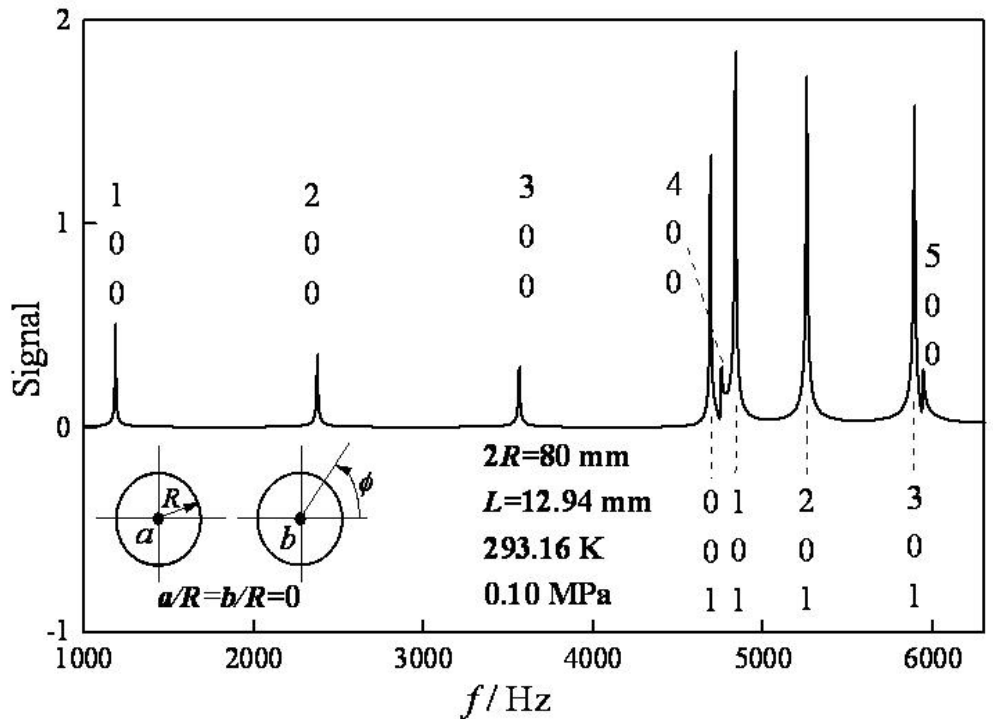

Fig. 3. Spectra for cylinder resonator at 1~6.5 kHz in argon when the source transducer is at $(r,\phi,z)=(0,0,0)$ and detector is at $(r,\phi,z)=(0,0,L)$

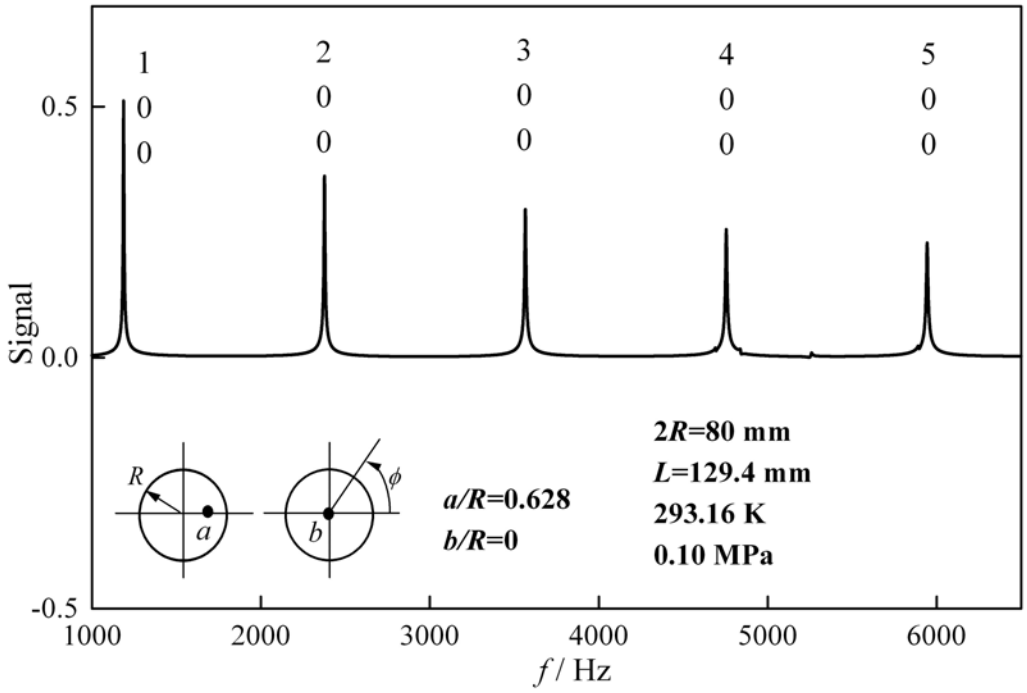

Fig. 4. Spectra for cylinder resonator at 1~6.5 kHz in argon when the source transducer is at $(r,\phi,z)=(0.628R,0,0)$ and detector is at $(r,\phi,z)=(0,0,L)$

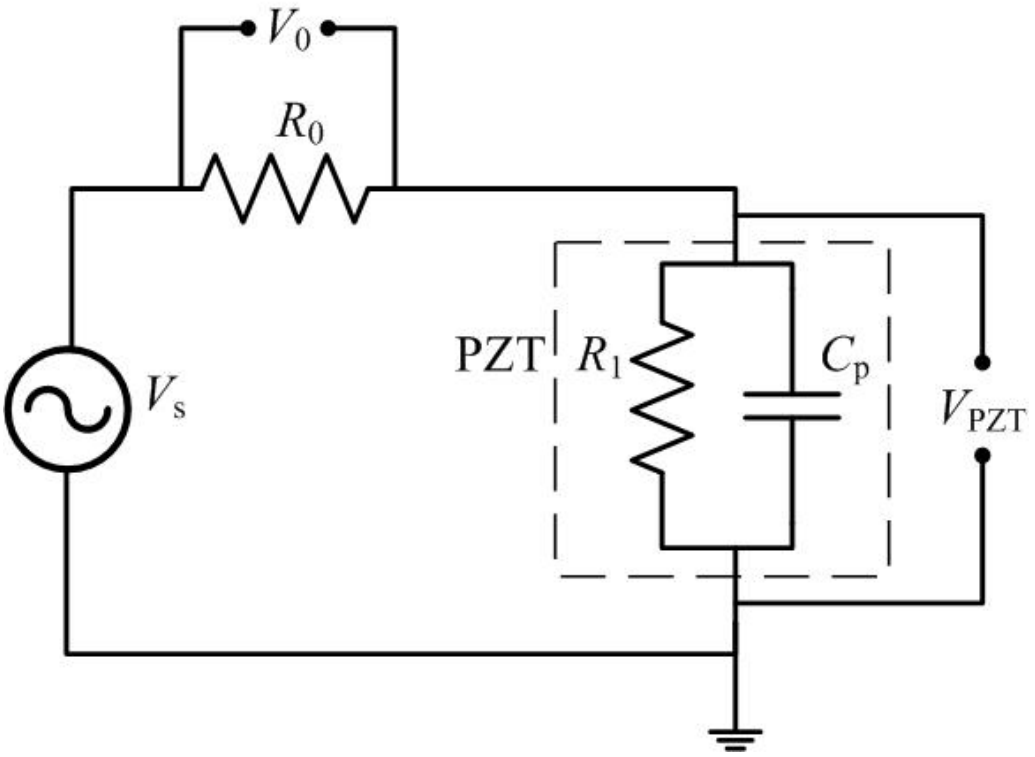

Fig. 5. Circuit used to measure the dissipation factor

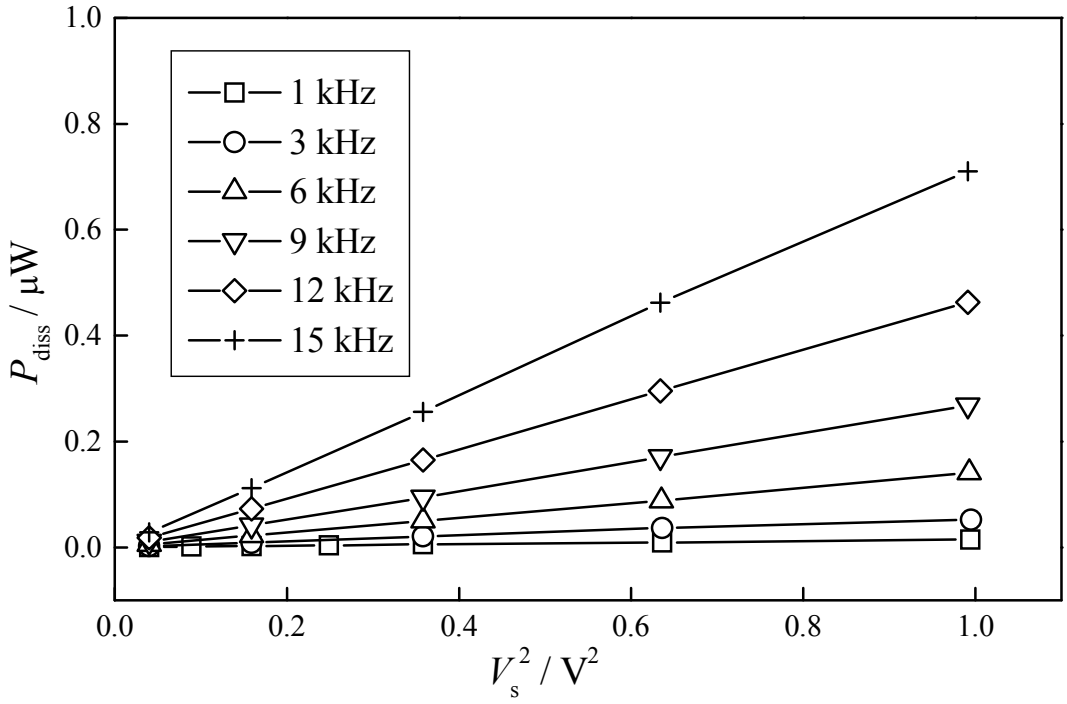

Fig. 6. Power dissipation of PZT 402 changing with the square of source voltage for different frequency

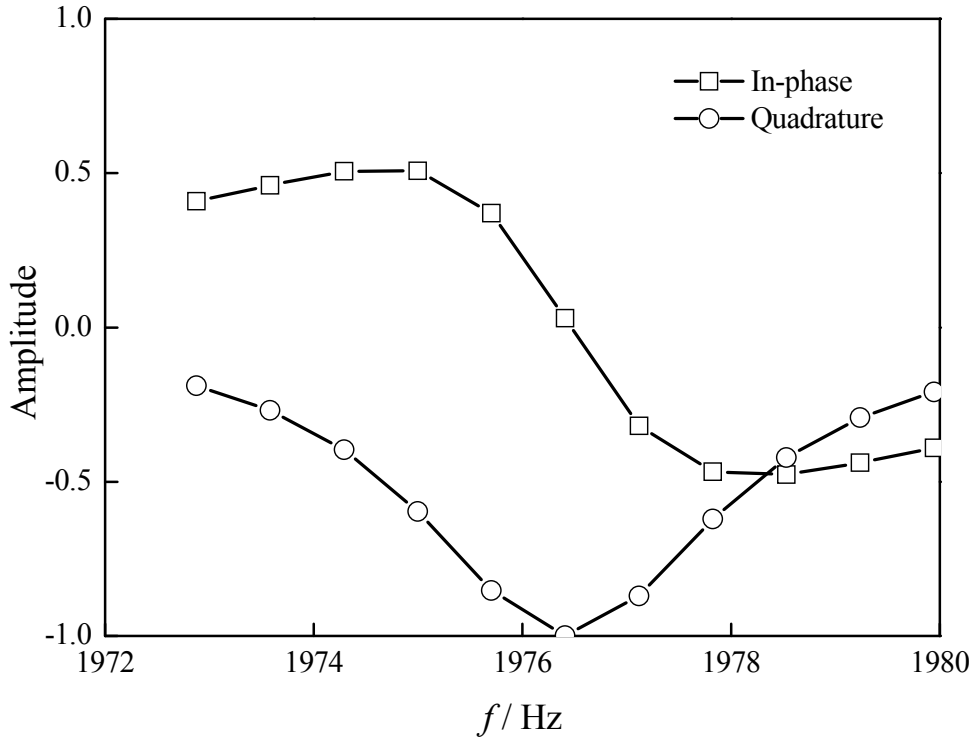

Fig. 7. The in-phase and quadrature voltages from the PZT detector as a function of frequency near the (100) longitude mode of cylinder resonator (2*R*=80 mm, *L*=80 mm) in argon.

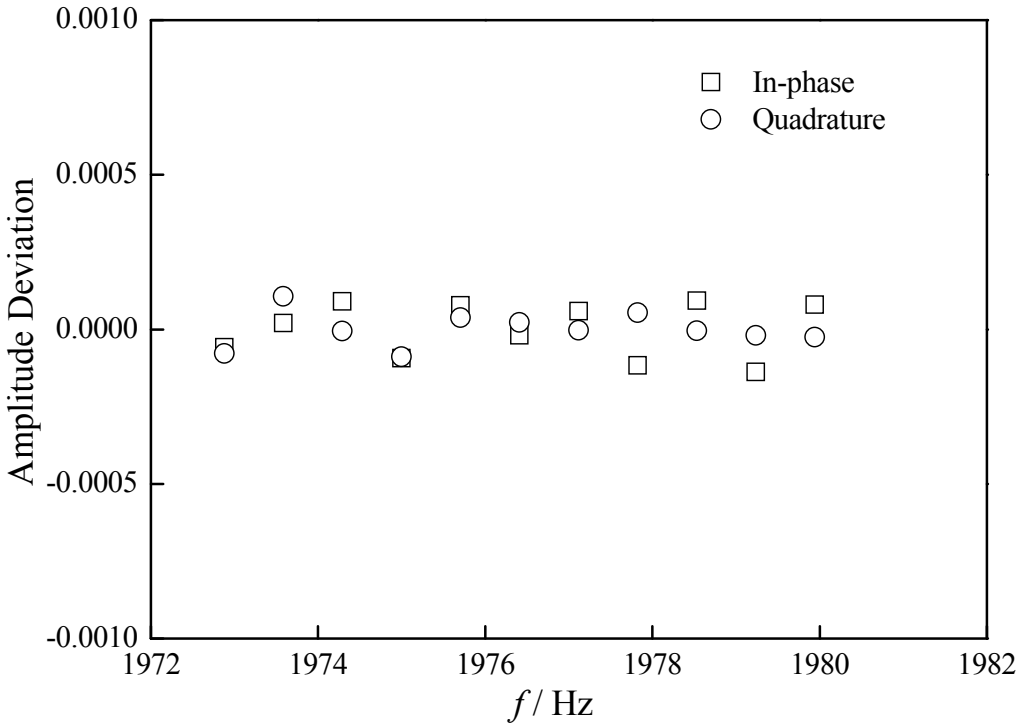

Fig. 8. Measured voltages minus calculated voltages[13]

Table 1 Properties of PZT 402

Name	Unit	Values
Radius	m	0.0032
Thickness	m	0.0004
Transverse charge coefficient d_{31}	$\times 10^{-12}\ \mathrm{m \cdot V^{-1}}$	-120
Transverse voltage coefficient g_{31}	$\times 10^{-3}\ \mathrm{V \cdot m \cdot N^{-1}}$	-10.8
Young's modulus	$\times 10^{10}\ \mathrm{N \cdot m^{-2}}$	7.6
Poisson ratio		0.31

Table 2 Perturbations for PZT and Microphone

	$\frac{\Delta f_{\mathrm{tr}}}{f_0} / 10^{-6}$	
	0.1 MPa	1 MPa
1/4 inch Microphone	-0.16	-1.60
PZT 402	-0.03	-0.27

Table 3 Results of the power dissipation measurement for PZT 402

f / Hz	V_0 / mV	V_{PZT} / V	V_s / V	tan δ	P_{diss} / μW
1000	0.236	0.199	0.199	0.002	0.0005
1000	0.354	0.299	0.299	0.003	0.0015
1000	0.472	0.398	0.399	0.003	0.0024
1000	0.590	0.498	0.499	0.003	0.0039
1000	0.708	0.597	0.598	0.003	0.0061
1000	0.943	0.796	0.797	0.003	0.0094
1000	1.179	0.995	0.997	0.003	0.0150
3000	0.707	0.199	0.199	0.004	0.0025
3000	1.414	0.398	0.399	0.003	0.0085
3000	2.121	0.597	0.598	0.003	0.0207
3000	2.826	0.797	0.798	0.003	0.0365
3000	3.533	0.995	0.997	0.003	0.0527
6000	1.411	0.199	0.199	0.004	0.0057
6000	2.824	0.398	0.399	0.004	0.0224
6000	4.235	0.597	0.598	0.004	0.0504
6000	5.641	0.795	0.797	0.004	0.0878
6000	7.051	0.994	0.996	0.004	0.1409
9000	2.117	0.199	0.199	0.005	0.0110
9000	4.234	0.397	0.399	0.005	0.0414
9000	6.351	0.596	0.598	0.005	0.0943
9000	8.451	0.793	0.796	0.005	0.1707
9000	10.565	0.992	0.996	0.005	0.2683

12000	2.821	0.198	0.199	0.006	0.0179
12000	5.646	0.397	0.399	0.006	0.0727
12000	8.467	0.595	0.598	0.007	0.1652
12000	11.260	0.792	0.796	0.007	0.2953
12000	14.073	0.990	0.995	0.007	0.4629
15000	3.529	0.198	0.199	0.008	0.0282
15000	7.061	0.396	0.399	0.008	0.1120
15000	10.592	0.594	0.598	0.008	0.2562
15000	14.084	0.790	0.796	0.008	0.4620
15000	17.606	0.988	0.996	0.008	0.7101